Molecular Insight into the Adsorption of H2S in the Flexible MIL-53(Cr) and Rigid MIL-47(V) MOFs: Infrared Spectroscopy Combined to Molecular Simulations

ARTICLE *in* THE JOURNAL OF PHYSICAL CHEMISTRY C · JANUARY 2011

Impact Factor: 4.77 · DOI: 10.1021/jp1092724

12 AUTHORS, INCLUDING:

Lomig Hamon
École des Mines de Nantes
21 PUBLICATIONS **1,099** CITATIONS
SEE PROFILE

Aziz Ghoufi
Université de Rennes 1
124 PUBLICATIONS **1,778** CITATIONS
SEE PROFILE

Gérard Férey
Université de Versailles Saint-Quentin
705 PUBLICATIONS **36,726** CITATIONS
SEE PROFILE

THE JOURNAL OF PHYSICAL CHEMISTRY C

ARTICLE

pubs.acs.org/JPCC

Molecular Insight into the Adsorption of H_2S in the Flexible MIL-53(Cr) and Rigid MIL-47(V) MOFs: Infrared Spectroscopy Combined to Molecular Simulations

Lomig Hamon,[†] Hervé Leclerc,[‡] Aziz Ghoufi,[§,∥] Laetitia Oliviero,[‡] Arnaud Travert,[‡] Jean-Claude Lavalley,[‡] Thomas Devic,[⊥] Christian Serre,[⊥] Gérard Férey,[⊥] Guy De Weireld,[†] Alexandre Vimont,[‡,*] and Guillaume Maurin[§,*]

[†]Thermodynamics Department, Faculté Polytechnique, UMONS, Place du Parc 20, 7000 Mons, Belgium

[‡]Laboratoire Catalyse et Spectrochimie, ENSICAEN, Université de Caen Basse Normandie, CNRS, 6 Bd du Maréchal Juin, 14050 Caen, France

[§]Institut Charles Gerhardt Montpellier, UMR 5253 CNRS-UM2-ENSCM, Université de Montpellier II, Place E. Bataillon, 34095 Montpellier Cedex 05, France

[∥]Institut de Physique de Rennes, UMR 6251 CNRS, Université Rennes 1, 263 Avenue du Général Leclerc, 35042 Rennes, France

[⊥]Institut Lavoisier, UMR CNRS 8180, Université Versailles-Saint Quentin en Yvelines, 78035 Versailles, France

Supporting Information

ABSTRACT: The adsorption of the acid gas H_2S has been explored in both MIL-47(V) and MIL-53(Cr) porous metal−organic frameworks (MOFs) by combining infrared measurements and molecular simulations. It is shown that while the MIL-47(V) structure remains rigid upon H_2S adsorption up to a pressure of 1.8 MPa, the MIL-53(Cr) solid initially present in the large pore form (LP) switches to its narrow pore version (NP) at very low pressure before undergoing a second structural transition from the NP to the LP versions at higher pressure. Such structural transitions further explain the different shape of the adsorption isotherms for both MILs. A further step consists of providing some insights into the microscopic arrangements of the adsorbate molecules within the pores of the MILs. At the initial stage of adsorption, the H_2S molecules mainly form hydrogen bonded species, either as hydrogen donor (in MIL-47 V) or hydrogen-acceptor (in MIL-53Cr) with the μ_2-O and μ_2-OH groups, respectively, present at the MOF surfaces. At higher pressure (1.8 MPa), the adsorbates are preferentially arranged within the channel in order to form dimers with a high orientational disorder. Both experimental and simulated adsorption enthalpies for H_2S decrease in the following sequence: MIL-53(Cr) NP > MIL-47(V) > MIL-53(Cr) LP. The conclusions drawn from this work are then discussed considering the use of such materials for the CH_4/H_2S separation by means of Pressure Swing Adsorption.

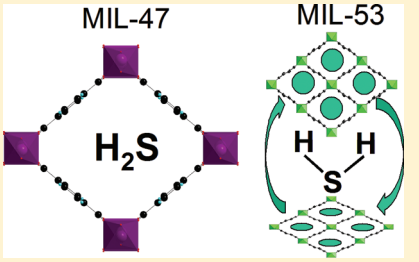

INTRODUCTION

The removal of CO_2 and H_2S from natural gas, coal/biomass gasification and reformate gas is of main interest in the use of gas and especially in the hydrogen production processes. CO_2 and particularly H_2S are harmful pollutants: H_2S can cause corrosion and usually damages the transition-metal used in fuel cells.[1] Acid gas recovery is also of great importance for the purification of both biogas (in which initial feed can contain 1−5% of H_2S) and natural gas (in which initial feed can contain some ppm up to 20% of H_2S). Moreover, regulations limit the amounts of sulfur species in fuels below 10−15 ppm. Sulfur compounds present in gases are commonly removed by gas−liquid absorption techniques in aqueous amine solutions. These processes are highly energy-greedy, the amine solutions being of very limited lifetime. Alternatively, adsorption processes such as PSA (Pressure Swing Adsorption) appear to be less energy demanding but the crucial point of such technology relies on selecting adsorbent material combining large adsorption capacity and good separation ability with a full regeneration at low energy cost. Chemisorption is one way to perform the gas separation of a mixture containing sulfur species[2] but this procedure needs specific reactivation of the adsorbents. Indeed, the physisorption appears to be the most suitable way to separate H_2S from syngas or natural gas as the adsorbent is expected to be more easily regenerable. Such a process usually allows for reaching a very low amount of sulfur compounds in feed. The Metal−Organic Frameworks (MOFs) materials can be very promising as adsorbents in order to capture sulfur compounds such as thiophene derivatives[3,4] and H_2S.[5] These materials combine metallic clusters with organic ligands showing in some cases zeolite topologies with higher microporous volumes and wider chemical

Received: September 28, 2010
Revised: November 26, 2010
Published: January 19, 2011

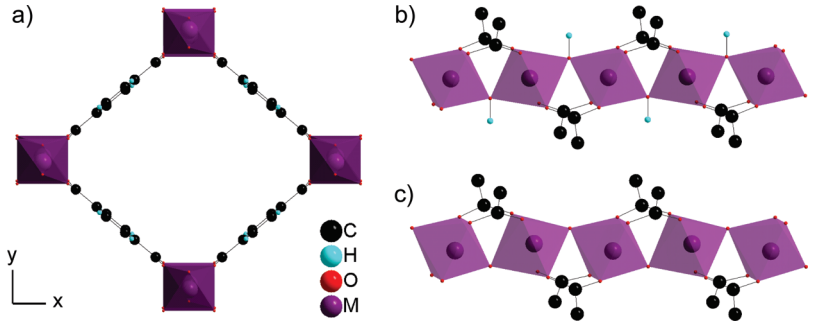

Figure 1. (a) View of the MIL-53(Cr) LP/MIL-47(V) structures along the chain (z axis), highlighting the 1D pores system with M = Cr^{3+} or V^{4+}. View perpendicular to the pores of the MIL-53(Cr) (b) and MIL-47(V) (c) with μ_2−OH and μ_2-O atoms linked to the Metal atom (M), respectively.

versatility. The present work aims at fully characterizing the H_2S adsorption phenomenon on two MOF materials, namely the MIL-47(V) and the MIL-53(Cr), presenting the same topology but containing two different metal centers. These solids are built-up from infinite chains of corner-sharing $CrO_4(OH)_2$ or VO_6 octahedra interconnected by terephthalate linkers[6−10] leading to the chemical formula M(X){$O_2C-C_6H_4-CO_2$} (X = O and M = V^{IV} for MIL-47(V) and X = OH and M = Cr^{III} for MIL-53(Cr)) (see Figure 1). Such an arrangement delimits a one-dimensional diamond-shaped pore system, with a Langmuir surface area comprised between 1400 and 1500 $m^2 \cdot g^{-1}$. The structure of the MIL-47(V) is actually known to remain unchanged upon the inclusion of any adsorbates, while the MIL-53(Cr) usually shows a spectacular breathing behavior upon various guest molecules including gases, vapors and drugs, corresponding mainly to a structural switching between a Large Pore and a Narrow Pore form.[6,7,9,11−15]

Following our previous study focused on the regenerability of MOFs after H_2S exposure,[5] these solids have been selected with two major criteria: (i) both show high stability and regenerability, and (ii) the shape of their H_2S adsorption isotherms significantly differs, behavior not explained so far. While the MIL-47(V) material shows a usual type I isotherm,[16,17] the so-obtained isotherm for the MIL-53(Cr) solid exhibits substeps as previously observed for other acid and polar gases.[5,6,16,17] From these results, one would suspect that MIL-53(Cr) also breathes in the presence of H_2S corresponding to a structural switching between a narrow and a large pore form, while MIL-47(V) does not undergo any structural modification. Such assumption will be discussed in light of the conclusions drawn from complementary in situ IR spectroscopy measurements and molecular simulations which allow exploring the phenomena at the microscopic scale. It will be emphasized how this joint experimental−theoretical approach can be a powerful tool to follow the structural behavior of MOFs upon adsorption when in situ X-ray diffraction is not available or hardly feasible in the case of a corrosive/harmful acid gas such as H_2S. Beyond the structural analysis of the MIL frameworks, a further step will consist of elucidating the arrangements and the energetics of H_2S in both MILs, highlighting the most significant differences observed depending on the cavity size (narrow pore vs large pore forms of MIL-53(Cr)) and the chemical composition of the MOF surface (large pore version of MIL-53(Cr) vs MIL-47(V)).

EXPERIMENTAL SECTION

Synthesis. MIL-53(Cr) and MIL-47(V) were synthesized on the gram scale and activated following previously reported procedures.[6,8] Experiments were directly carried out on the powdered sample (particles size within the micrometer range).

Gravimetric Measurements. The adsorption experiments were carried out at 303 K up to a H_2S pressure of 0.9 p/p_{sat} (2.03 MPa) using a commercial gravimetric adsorption device (Rubotherm Präzisionmesstechnik GmbH) which avoids subcritical gas condensation.[18−23] Prior to each measurement, the MOF sample was outgassed at 393 K, under secondary vacuum (10^{-3} Pa) until the mass was invariant (weight variation < 50 μg). H_2S purity was 99.5% (provided by Praxair Belgium). The buoyancy effect of the gas phase on the adsorbent volume was then corrected to determine the excess adsorbed mass. The gas phase density was determined using an appropriate equation of state (EOS); the adsorbent volume was evaluated by a direct helium buoyancy effect measurement assuming that helium does not adsorb.[24] The helium density was determined using a modified Benedict−Webb−Rubin EOS.[25] A maximum 5% error bar was evaluated for the adsorbed amounts. EOS used for buoyancy effect correction is of Helmholtz type.[26]

The reported experimental data correspond to absolute adsorption amounts obtained from the correction of the primary excess values via the following expression (eq 1):

$$n^a = n^\sigma + \rho_g V_p \quad (1)$$

where n^a and n^σ are the absolute and excess amounts adsorbed, respectively, and V_p is the micropore volume of the two samples estimated from nitrogen physisorption at 77 K. The measured gas density ρ_g is included to correct gas nonideality for the experiments performed at high pressure.

The isosteric heats of adsorption have been determined for all MILs following the procedure previously described.[27]

Infrared Spectroscopy. A small amount of sample (2 mg) was dispersed in deionized water and spread on a silicon wafer for IR measurements during H_2S adsorption. They were placed in a quartz cell equipped with KBr windows. A movable quartz sample holder allows adjustment of the pellet in the infrared beam for spectra acquisition and to displace it into a furnace at the top of the cell for thermal treatments. The cell was connected to a vacuum line for evacuation, calcination steps ($p_{residual} = 10^{-3}-10^{-4}$ Pa) and for the introduction of H_2S into the infrared cell.

H_2S has a high degree of purity (99.5%, provided by Air Liquide). Note that traces of COS have been detected in H_2S by the characteristic infrared band situated at 2060 cm^{-1}. H_2S was adsorbed either at room temperature or at about 220 K in order to increase the adsorbed amount since the setup does not allow introduction of H_2S at a pressure above 100 kPa. Spectra were further recorded at these two temperatures. In the low temperature adsorption experiments, the pellet was brought to 220 K by cooling the sample holder with a mixture of dry ice and octane,

Table 1. Force Field Parameters for Both MIL-47(V) and MIL-53(Cr) Frameworks and H_2S

atom type	σ_{ii} (Å)	ε_{ii} (eV)
o_c	3.12000	0.002600
μ_2-o	3.12000	0.002600
h_o	0.00000	0.000000
cg1/cg2/c_c	3.48000	0.004160
h_c	2.82000	0.000660
Cr	2.69000	0.000650
V	2.80000	0.000700
S	3.72000	0.020025

after quenching the sample from the thermal treatment temperature. The pressure of H_2S inside the IR cell was measured by a pressure gauge (10^{-1}−10^4 Pa range). Transmission IR spectra were recorded in the 500−5600 cm^{-1} range, at 4 cm^{-1} resolution, on a Nicolet Nexus spectrometer equipped with an extended KBr beam splitting device and a mercury cadmium telluride (MCT) cryodetector.

MODELING

Microscopic Models and Force Fields. The periodic models of the MIL-47(V) and the LP form of MIL-53(Cr) were built using the atomic coordinates previously reported.[7,8] As the NP structure of the MIL-53(Cr) upon H_2S adsorption was not solved by X-ray diffraction, we considered a predicted one in presence of a 4 H_2S molecule/u.c., loading that mimics the experimental adsorbed amount of H_2S at saturation for this form. For this purpose, we followed the same NσT Molecular Dynamics strategy to consider the size and shape changes of the framework, we successfully employed in the case of CO_2,[28] based on the previously reported intramolecular terms for the MIL-53(Cr) framework while the intermolecular contributions of the adsorbate/adsorbent interactions were treated as described below. All of the details of such simulation can be found in our previous paper.[28] The so-generated structure was then considered as an "average" one that can fairly represent the NP form in the whole range of pressure investigated in this structure. This approach assumes that the volume of the NP form only slightly changes when the loading increases as we have previously shown in the case of CO_2 with a cell volume expansion between 2.2 and 4 CO_2/u.c. of less than 3%.[28] It thus leads to a NP structure with the following unit cell parameters a = 19.10 Å, b = 9.27 Å, c = 6.69 Å, β = 95.50° (space group $C2/c$) corresponding to a cell volume of 1140 $Å^3$ slightly larger than those observed for CO_2.[14]

The intermolecular interactions were considered as follows: the set of Lennard−Jones (LJ) parameters for describing the MIL-53(Cr) and MIL-47(V) frameworks was created by combining the generic Universal Force Field[29] for the inorganic part of the crystalline lattice (the metal center with its oxygen environment) and the Dreiding interatomic potential for the organic part.[30] The corresponding LJ parameters are summarized in Table 1, the location of each atom type on the framework being reported in Figure 2. The partial charges carried by the atoms of both MIL frameworks were further taken from our previous studies based on DFT calculations.[31,32]

H_2S was represented by the three-site model reported previously by Kamath et al.[33] Such a model has successfully been used to reproduce the experimental vapor−liquid phase equilibrium data. The corresponding partial charges expressed in electron units are 0.19 and −0.38 for the H and S atoms, respectively. The LJ term is centered only on the sulfur nucleus with corresponding parameters reported in Table 1.

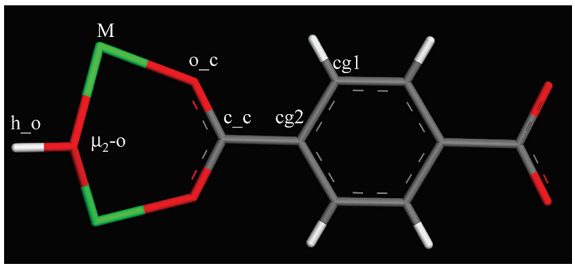

Figure 2. Labels of the atoms for the organic and inorganic parts for both MIL-53 (Cr) and MIL-47 (V) materials corresponding to the forcefield atom types (M = V or Cr), to allow the easy reading of Table 1.

The adsorbate/MIL-framework interactions were then treated via both Coulombic and LJ interactions. The LJ parameters corresponding to the interactions between H_2S and each atom of both MIL frameworks were obtained by combining the LJ parameters of the S nucleus with that considered from the forcefield describing the MILs, using Lorentz−Berthelot mixing rules.

Grand Canonical Monte Carlo-Monte Carlo Simulations. Absolute adsorption isotherms were computed at 303 K in both MILs using Grand Canonical Monte Carlo (GCMC) simulations. The structures of MIL-47(V) and both NP and LP forms of MIL-53(Cr) were treated rigid and the periodic conditions were employed. The simulation box consisted of 16 (2 × 2 × 4) unit cells for the orthorhombic MIL-47(V) structure while 32 (2 × 4 × 4) unit cells were considered for both orthorhombic LP and monoclinic NP forms of MIL-53(Cr). A typical GCMC run consisted of 3×10^8 Monte Carlo steps, each step considering randomly selected moves of H_2S molecules with fixed probabilities, e.g., translation (0.2), rotation (0.2) and insertion/deletion (0.6). The chemical potentials for H_2S were calculated with the Widom insertion method from the NpT ensemble.[34] The electrostatic contributions were estimated using the Ewald summation while the short-range interactions were truncated at a *cutoff* distance fixed at 12 Å. Finally, the adsorption enthalpy at low coverage was computed for all MILs through a biased Widom's test particle method recently reported.[35]

In order to explore the preferential arrangements of H_2S in the three different considered MILs, additional Monte Carlo (MC) simulations were run in the canonical ensemble (NVT), for a fixed number of H_2S molecules per unit cell close to those experimentally obtained at the plateau of the isotherms for each MIL form. Both radial distribution functions corresponding to the guest/host and guest/guest pairs and the probability densities of H_2S within the pores were calculated from the analysis of the configurations stored during the canonical MC runs.

Analytical (NP, LP) MIL-53(Cr) Phase Mixture Model. If one assumes that the two structural NP and LP forms contribute to the adsorption process, then the experimental adsorption isotherm can be described in the whole range of pressure by the eq 2:

$$N(p) = X_{NP}(p)N_{NP}(p) + (1 - X_{NP}(p))N_{LP}(p) \qquad (2)$$

where for a given pressure (p), N represents the total H_2S adsorbed amount, X_{NP} and X_{LP} are the fractions of the NP and LP forms, respectively, assuming that the $X_{LP} = 1 - X_{NP}$, N_{NP}, and N_{LP}

dx.doi.org/10.1021/jp1092724 |J. Phys. Chem. C 2011, 115, 2047–2056

correspond to the H_2S adsorbed amounts in the NP and LP forms, respectively.

A Langmuir-type equation (eq 3) can be then considered to model the gas adsorption for both NP and LP forms.

$$N_i(p) = \frac{pK_i}{1+\frac{pK_i}{N_i^{sat}}} \text{ with } i = \text{LP, NP} \quad (3)$$

where K_i corresponds to the Henry constant, N_i^{sat} is the H_2S adsorbed amount obtained at the first (NP) and the second (LP) plateau of the adsorption isotherm for the NP and LP forms, respectively.

Equation 2 can then be rewritten as follows (eq 4):

$$N(p) = X_{NP}(p)\left[\frac{pK_{NP}}{1+\frac{pK_{NP}}{N_{NP}^{sat}}}\right] + (1-X_{NP}(p))\left[\frac{pK_{LP}}{1+\frac{pK_{LP}}{N_{LP}^{sat}}}\right] \quad (4)$$

Indeed, as the Henry constants K_i, and the saturation capacities N_i^{sat}, are obtained experimentally for both NP and LP forms, one can extract the fractions X_i (i = NP and LP) as a function of the pressure by fitting the adsorption isotherm using eq 4.

RESULTS AND DISCUSSION

Figure 3, parts a and b, reports the hydrogen sulfide adsorption isotherms of the MIL-47(V) and the MIL-53(Cr) solids at 303 K for pressures up to 1.8 MPa with a zoom area for low pressures up to 60 kPa for the MIL-53(Cr) (insert in Figure 3c). The MIL-47(V) exhibits a usual monotonic quasi-type I shape isotherm according to IUPAC classification: an initial Henry domain for pressure below 25 kPa (with a constant of 47.0 mmol·g^{-1}·MPa^{-1}) and a second linear zone for pressure up to 30 kPa (with a slope of 80.7 mmol·g^{-1}·MPa^{-1}). The saturation capacity for this material is 14.6 mmol·g^{-1}. In contrast, the profile of the adsorption isotherm is more complex for the MIL-53(Cr) solid: after a quasi Henry region for pressure below 3.5 kPa with a constant of 78.9 mmol·g^{-1}·MPa^{-1}, a first increase is observed with a maximal slope of 597.7 mmol·g^{-1}·MPa^{-1} prior to reaching a plateau corresponding to a saturation capacity of 3.7 mmol·g^{-1}. The second step then starts at 118 kPa and shows a maximum slope of 28.7 mmol·g^{-1}·MPa^{-1}, the saturation capacity being 13.1 mmol·g^{-1}.

Infrared measurements have been further performed to explore the adsorption modes of H_2S in both MILs. The corresponding spectra were first recorded at 298 and 220 K in the 0−40 kPa H_2S pressure domain (see insets in Figure 4, parts a and b, respectively). They display weak bands in the 2500−2600 cm^{-1} range assigned to the ν(SH) bands of the adsorbed H_2S species. The plots of the integrated intensity of these bands in the 2500−2600 cm^{-1} range vs the pressure introduced into the cell at 220 K, are reported in Figures 4 and the Supporting Information for data relative to the adsorption at 298 K. The optical isotherm for MIL-47(V) obtained from the spectra recorded at 220 K (Figure 4a) shows an I-type adsorption isotherm, similar to that deduced from the gravimetric measurement. Similarly, the optical isotherm of MIL-53(Cr) (Figure 4b) is analogous to that obtained from the gravimetric measurements described above: a very fast uptake occurring at low pressure (0.5 kPa at 220 K, 40 kPa at 298 K) is followed by a first plateau ranging from

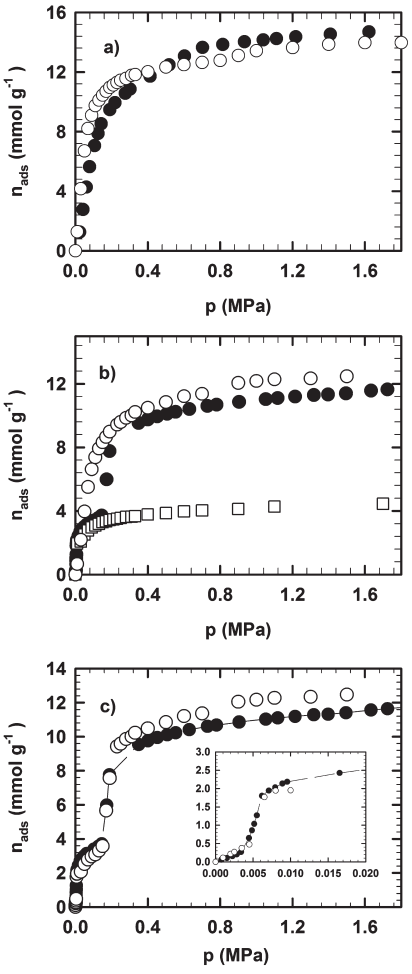

Figure 3. Adsorption isotherms of H_2S in MIL-47(V) (a) and in MIL-53(Cr) (b,c) at 303 K in the whole range of pressure: gravimetry (full symbols), simulations (empty symbols) from the rigid NP (square symbols) and LP (circle symbols) (b) and from the composite approach (c). Insert on (c) provides a comparison between gravimetry and simulations in the low pressure domain.

0.5 kPa to around 2 kPa at 220 K. At higher pressure (2−3 kPa at 220 K), one observes a second sudden uptake which then results in a final step.

In order to provide further insights into the origins of the different shapes of the optical and gravimetric isotherms, further examination of the IR spectra is required. Previous combined in situ X-ray diffraction and IR studies on the MIL-53(Cr)/CO_2 system[6] have shown that the LP and NP configurations of the MIL-53(Cr) are characterized by distinct infrared bands of the terephthalic entities (ν18a ring mode), located at 1022 cm^{-1} and 1017 cm^{-1} for the LP and NP structures of the MIL-53(Cr), respectively. Following the conclusions drawn from this previous investigation, the intensity of the 1022 and 1017 cm^{-1} bands versus the applied p(H_2S) from the spectra collected during the adsorption process at 220 K, were plotted. This plot, represented in Figure 5b, shows that the intensity of the ν18a ring mode centered at 1022 cm^{-1} for the dehydrated MIL-53(Cr) sample strongly decreases in intensity in favor of the band at 1017 cm^{-1} during the first H_2S uptake. This behavior indicates that the material initially present in its LP form switches to the NP configuration at the initial stage of H_2S adsorption, the solid being fully converted into the NP form when the first plateau is

dx.doi.org/10.1021/jp1092724 |J. Phys. Chem. C 2011, 115, 2047–2056

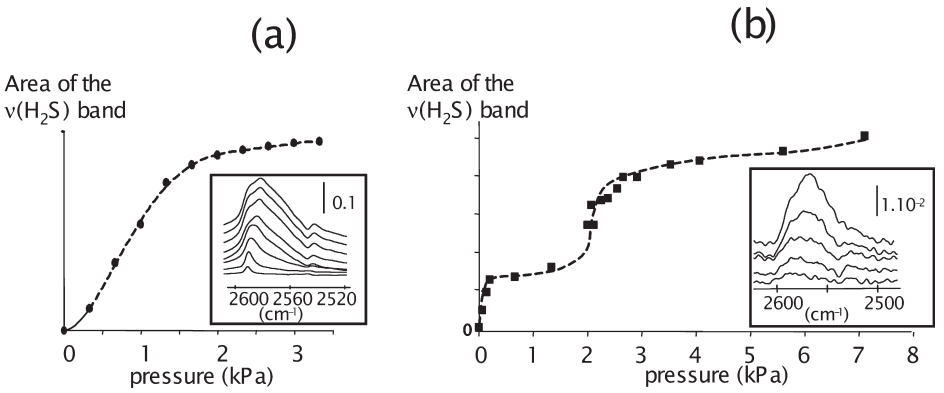

Figure 4. Variation of the areas of the $\nu(H_2S)$ band versus the H_2S pressure introduced into the cell at 220 K for MIL-47(V) (a) and MIL-53(Cr) (b). Insets: Infrared spectra in the $\nu(H_2S)$ range.

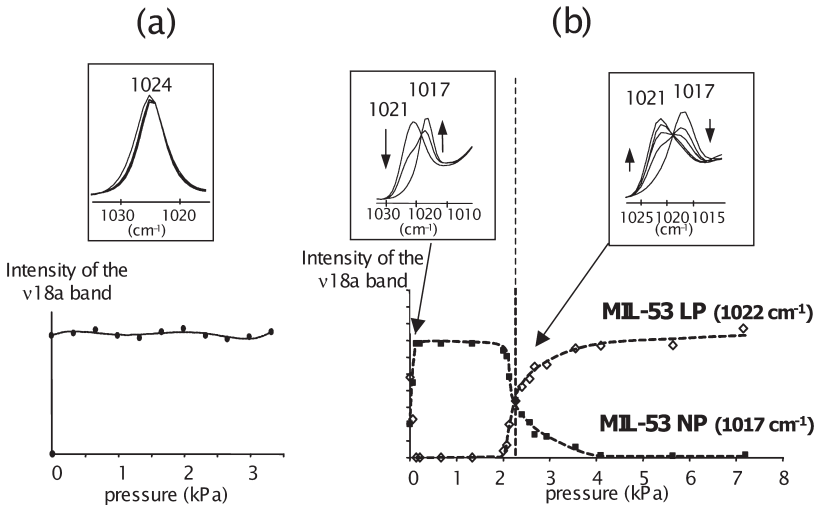

Figure 5. Adsorption of H_2S in MIL-47(V) (a) and in MIL-53(Cr) (b) at 298 K. Intensity of the $\nu(18a)$ mode in function of the pressure introduced (bottom). Insets: spectra of the $\nu 18a$ band recorded upon H_2S pressure.

reached. During the second uptake ($p(H_2S)$ varying from 2 to 3 kPa), the reverse phenomenon occurs: the $\nu 18a$ band at 1017 cm^{-1} (NP form) decreases in favor of the band at 1022 cm^{-1} (LP form), revealing that the sudden increase in H_2S loading is correlated to the reopening of the structure.

Figure 5a shows the corresponding spectra obtained during H_2S adsorption on the MIL-47(V). In this case, the position of the $\nu 18a$ band (1024 cm^{-1}) does not significantly change during the whole H_2S adsorption process. Hence, the absence of any characteristic step in the optical isotherm reveals that the structure remains unchanged during the whole H_2S adsorption. This is in agreement with what has previously been shown with various gases.[17,32] To confirm such experimental findings, GCMC simulations were first performed using a rigid MIL-47(V) framework. As can be seen in Figure 3a, the simulated data agrees reasonably well with the gravimetry measurements for both shape and amounts of adsorbed H_2S in the whole range of pressure which allows us (i) to confirm that this structure is not expected to undergo any significant structural modification upon adsorption and (ii) to validate the force field used to describe the host/guest interactions. For the more complex MIL-53(Cr) solid, our analytical phase mixture model was first employed to check whether the experimental adsorption isotherm can be reproduced by assuming that the global isotherm can be decomposed into two contributions from the NP and the LP forms, respectively. As shown in Figure 6a, the use of eq 4 using Henry's constants and the saturation capacities determined by gravimetry, allows us to match the experimental adsorption isotherm in the whole range of pressures quite well, confirming that the presence of substeps in the very low (~4 kPa) and intermediate (~200 kPa) domains of pressure can be attributed to consecutive structural transitions. The resulting modeled fractions of the NP and LP forms were then extracted as a function of the pressure (see Figure 6b). The so-obtained profile clearly shows that the MIL-53(Cr) initially present in its LP form switches to the NP version in a pressure range centered around 4 kPa prior to return to the LP form at a higher pressure around 200 kPa. One can observe that the domains of existence of the pure NP version lies between 12 and 136 kPa, while the coexistence of the NP and LP forms span in a much narrower range of pressures.

The following step thus consisted of constructing the simulated composite isotherm from the isotherms calculated individually in both rigid NP and LP forms (see Figure 3b), using eq 2. The composite adsorption isotherm was then compared with the experimental one in Figure 3c. One observes a very good agreement between the simulated and experimental adsorption isotherms even in the low domain of pressure, which

dx.doi.org/10.1021/jp1092724 |J. Phys. Chem. C 2011, 115, 2047–2056

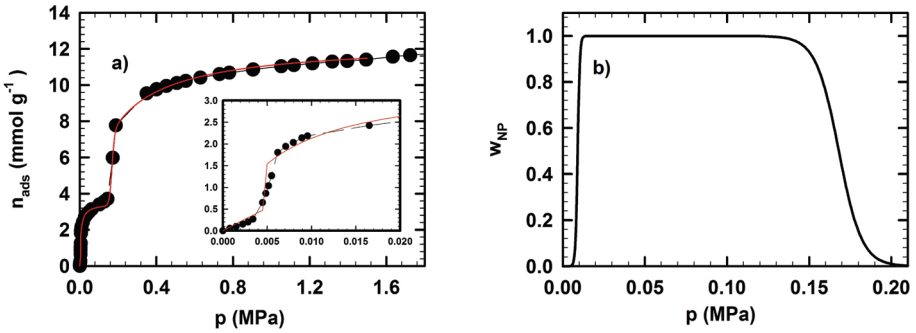

Figure 6. (a) Fit of the experimental adsorption isotherm of H_2S in MIL-53(Cr) at 303 K using eq 4 (insert reports the low pressure domain). (b) The so-extracted fraction of the NP form of MIL-53(Cr) for the whole range of pressure.

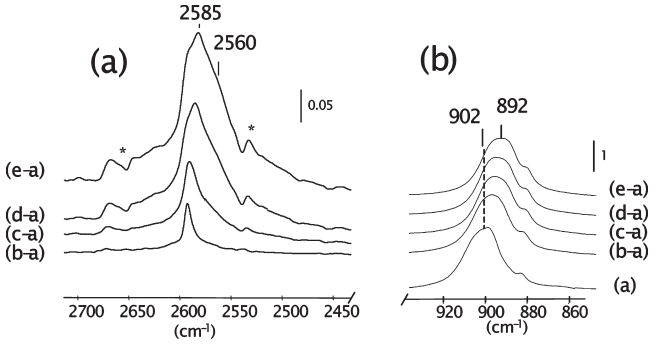

Figure 7. Infrared spectra of MIL-47(V) outgassed at 423 K under secondary vacuum (a) followed by introduction of increasing equilibrium pressure of H_2S at 220 K ($p(H_2S)$ = 220 Pa (b), 340 Pa (c), 530 Pa (d), and 1,2 kPa (e). Part a: focus on $\nu(H_2S)$ range. Inset b: focus on $\nu(V=O)$ range.

allows us to validate both the forcefield for describing the H_2S/MIL-53(Cr) framework interactions and the analytical phase mixture model.

A further step consisted of probing the host−guest interactions in both MILs. The spectrum of the activated MIL-47(V) sample does not present any ν(OH) band in the 3400−3800 cm^{-1} range but displays a strong band at 902 cm^{-1} (Figure 7b(a)). This band, not perturbed upon H/D exchange, is therefore assigned to the $\nu(V=O)$ mode of the asymmetric V−O−V bond sharing two consecutive VO_6 octahedra. It is worth noting that its wavenumber shifts toward lower values when the solid is exposed to H_2S. Such a downward shift has been reported for R−H...O = V complexes in Argon matrix (R = Cl).[36] We therefore propose the formation of the following adduct V = O···H−S−H, in which H_2S plays the role of an acidic molecule. It corresponds to the ν(SH) band at 2592 and 2585 cm^{-1} in these species.

Alternatively, hydrogen bonded species involving H_2S and π electrons of the aromatic ring could be also considered since the asymmetric ν(SH) mode in the spectrum of H_2S in liquid solvent such as benzene, toluene, and xylene gives rise to a band at 2582−2585 cm^{-1}.[37] At higher H_2S pressure, a shoulder appears at 2560 cm^{-1}. The position of this ν(SH) band is close to the one observed in the spectrum for oligomeric H_2S species in Ar matrix.[38] This observation suggests the formation of a liquid-like phase inside the channel of the MIL-47(V).

Molecular simulations performed for the MIL-47(V) system at a loading of 10 H_2S molecules per unit cell, confirm these experimental findings. One can observe from the radial distribution function (rdf) plotted for the $H(H_2S)-O(\mu_2\text{-}O)$ pair in Figure 8a that there is a distinct peak centered at a distance of 2.15 Å characteristic of a predominant interaction between the proton of H_2S and the μ_2-oxygen atoms of the MIL-47(V) framework. Such a relatively strong interaction is consistent with the high adsorption enthalpy values of 27.1 and 29.5 kJ·mol^{-1} estimated from the simulations and the isosteric method, respectively. This main interaction is illustrated in Figure 9a, which reports a typical arrangement of H_2S in the MIL-47(V) at high loading. Our simulations also evidence that additional interactions can occur between H_2S and the phenyl rings of the organic linkers (see Figure 9a). The rdf for the $H(H_2S)-S(H_2S)$ pair was further compared to those calculated for H_2S in the liquid state (Figure 8b) in order to highlight the effect of the confinement on the arrangement of the H_2S molecules. One observes that the first peak is shifted to shorter distances, suggesting that the hydrogen bonds between H_2S are slightly stronger when the hydrogen sulphide molecules are confined within the pores of the MIL-47(V) form. Further, it was found that the number of hydrogen bonds evaluated using the criteria previously reported,[39] is the same as in the liquid state (see Table 2). Figure 9a also shows that the weakly bonded H_2S molecules are arranged in such a way to form dimers, consistent with a liquid-like behavior. One should notice that these molecules are characterized by a rather high orientational disorder within the channel.

In addition to two weak ν(OH) bands at 3610 and 3580 cm^{-1}, the spectrum of MIL-53(Cr) activated at 473 K displays two bands at 3654 and 924 cm^{-1} assigned to ν(OH) and δ(OH) mode, respectively, for the μ_2-hydroxyl groups bridged over two chromium atoms[11] (Figure 10a). Introduction of H_2S into the cell at room temperature (pressure from 4 to 33.3 kPa) perturbs both bands: the ν(OH) band broadens and downward shifts from 3654 to 3490 cm^{-1}, whereas the δ(OH) band upward shift from 924 to 980 cm^{-1} (Figures 10b−e). Such perturbations characterize the formation of H-bonded complex Cr−OH···SH_2 in which the hydroxyl group and the sulfur atom of H_2S plays the role of H-donor and H-acceptor, respectively. The magnitude of the ν(OH) band shift ($\Delta\nu$(OH)) can be related to the acidity of the hydroxyl groups: the higher the shift, the stronger the acidity. In the present case, the measured $\Delta\nu$(OH) is 164 cm^{-1}, a lower value than the one reported for H-bonded complexes between H_2S and silanol groups of silica (210−240 cm^{-1})[40] or bridged hydroxyls in MFI zeolite (∼600 cm^{-1}).[41] One can thus conclude that the Brønsted acidity of the Cr−OH groups present in the MIL-53(Cr) solid is very low, in agreement with previous results relative to the acidity measurements using CD_3CN and CO as probe molecules.[11] Further, the presence of adsorbed H_2S species is evidenced in the spectra (Figure 10) by two ν(SH) bands at 2575 and 2585 cm^{-1} which intensity increase is

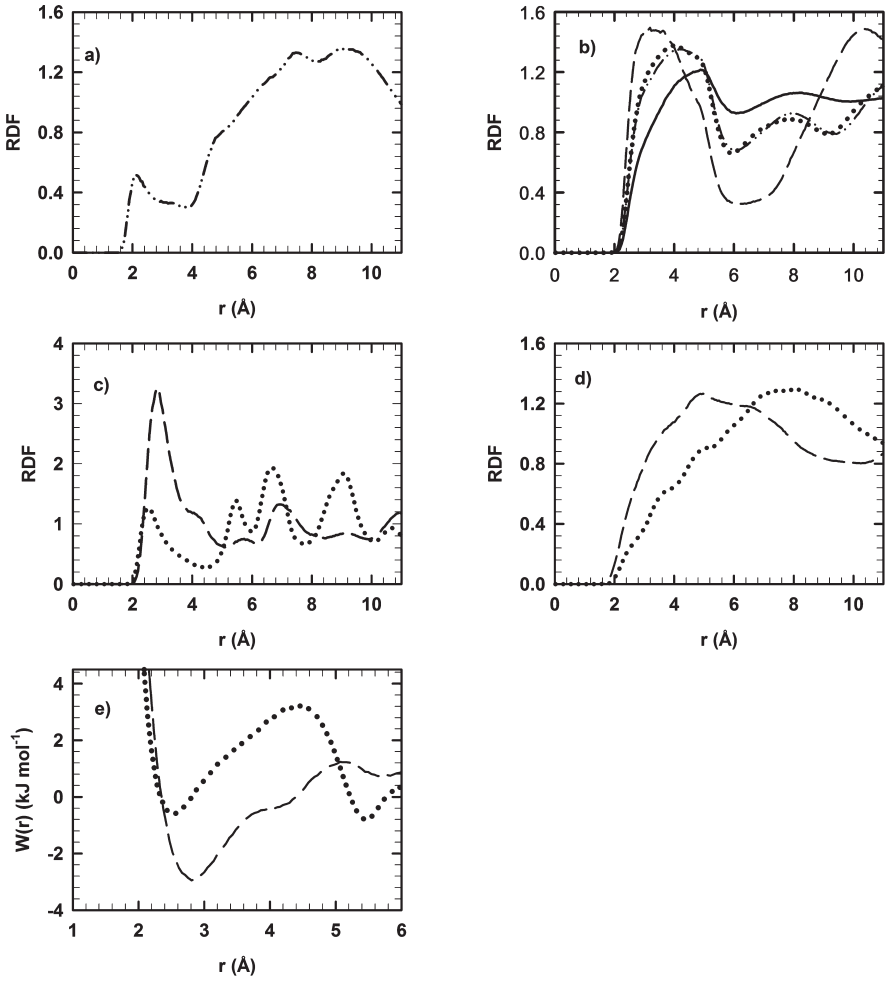

Figure 8. Radial distribution functions (rdf) calculated from the Monte Carlo simulations at 303 K for the different pairs: H(H_2S)−μ_2-O (c) (a), H(H_2S)−S(H_2S) (b), S(H_2S)−H(μ_2-OH) (c), and H(H_2S)−O(carboxylate) (d) for MIL-53(Cr) NP (dash lines), MIL-53(LP) (dot lines), MIL-47(V) (dash dot lines), and liquid phase (solid lines). Free energy profiles corresponding to the S(H_2S)−H(μ_2-OH) interactions in both NP and LP forms (e).

related to the decrease of the δ(OH) feature (see SI, Figure SI1). The two SH bands are thus assigned to the νs and νas modes of H_2S in the 1:1 complex with the Cr−OH group. When $p(H_2S)$ reaches 40 kPa, all of the Cr−OH groups are perturbed and the thermogravimetric measurements performed in the same conditions indicate that the adsorbed amount of H_2S (around 3−3.1 mmol·g^{-1}) is slightly lower than the concentration of the structural Cr−OH groups present in a perfect MIL-53(Cr) structure (3.7 mmol·g^{-1}). One can conclude that the 1:1 Cr−OH:H_2S complex corresponds to the most predominant adsorption mode appearing during the first uptake and that the adsorbed amount of H_2S at the first plateau (NP form) should depend on the number of free Cr−OH groups present in the sample. Further, one also notes a low asymmetric tail occurring from 2570 to 2520 cm^{-1}. The observation of such a low frequency component suggests that, in addition to the H bonded complex between H_2S and the Cr−OH groups, hydrogen bonds due to H_2S−H_2S interactions are also present.

In the spectrum of MIL-53(Cr) recorded after the second uptake (Figure 10f−a), the intensity of the low wavenumber ν(SH) component at 2565 cm^{-1} is more intense whereas the δ(OH) band is no more perturbed (Figure 10 right). In this condition, the ν(OH) band is observed at 3525 cm^{-1} and the δ(OH) one at 975 cm^{-1}. The corresponding $\Delta\nu$(OH) shift of 130 cm^{-1} is significantly lower in the NP structure (164 cm^{-1}, Figure 10a−e), showing that the strength of the hydrogen bond between the H_2S and Cr−OH group is significantly weaker in the LP form. Theses results indicate that at high loading, the strength of the interaction between H_2S and Cr−OH groups of the LP form is decreased as compared to the NP form. As suggested by the increase of the low ν(SH) component at 2565 cm^{-1}, this phenomenon could result from the condensation of H_2S molecules in the pores of the LP form. The stronger interaction in the NP form can be explained by the confinement of H_2S induced by the closer proximity of the cavity wall in this configuration.

Molecular simulations further bring some insights into the microscopic arrangements of H_2S and their predominant interactions with both the NP and LP forms of the MIL-53(Cr) solid. In a first step, one explored the preferential adsorption sites for H_2S in the NP form when the first plateau is reached, e.g., for almost 4 guest molecules per unit cell. The rdf calculated for the S(H_2S)−H(μ_2-OH) pair (Figure 8c) clearly confirms the presence of weak hydrogen bonds between the protons of the μ_2-OH group and the sulfur atoms of the adsorbed H_2S with a mean characteristic S(H_2S)−H(μ_2−OH) distance of 2.71 Å. The integration of this rdf plot shows that all of the μ_2-OH groups are involved in the interactions with H_2S via the formation of 1:1 complex. Furthermore, the rdf for the H(H_2S)−S(H_2S) pair

dx.doi.org/10.1021/jp1092724 |J. Phys. Chem. C 2011, 115, 2047–2056

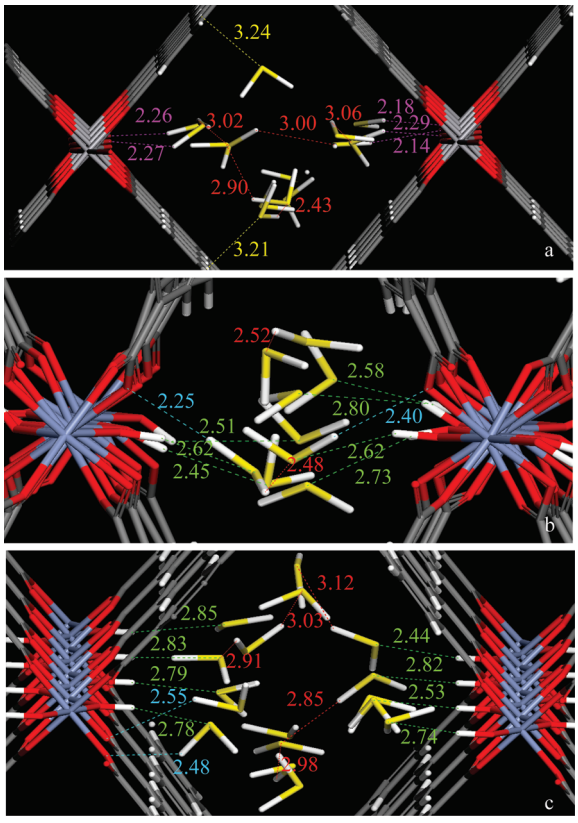

Figure 9. Illustrations of the preferential arrangements for H_2S simulated at 303 K in MIL-47(V) (a), MIL-53(Cr) NP (b) and MIL-53(Cr) LP (c) solids. The distances are reported in Å: $S(H_2S)-O(\mu_2\text{-OH})$ in green, $H(H_2S)-S(H_2S)$ in red, $H(H_2S)-O((\mu_2\text{-O})$ in purple, $S(H_2S)-O$-(carboxylate) in light blue and $S(H_2S)-H$(phenyl) in yellow.

Table 2. Results of Hydrogen-Bond Analyses for H_2S in the MILs and in the Liquid State

no. of H bonds	liquid	MIL-53(NP)	MIL-53(LP)	MIL-47(V)
	0.10 (0.08[a])	0.11	0.10	0.10

[a] According to ref 39.

evidence that the hydrogen bonds between the hydrogen sulfide molecules are slightly stronger when they are confined within the pores of the NP structure than in the MIL-47(V) form as shown by a shift of the first peak to smaller distances while only a slightly higher average number of hydrogen bonds is observed compared to the liquid state (see Table 2). One should notice that the so-obtained hydrogen bonds are much weaker than those previously pointed out for H_2O in the same MIL-53(Cr) solid.[13] A further analysis shows that the H_2S molecules are arranged within the channel in such a way to preferentially form dimers with a high orientational disorder as shown in MIL-47(V). This host/guest geometry again significantly differs with the one obtained for H_2O, where a highly ordered arrangement was pointed out. In addition to their interactions with the organic linkers as seen in MIL-47(V), H_2S tends also to significantly interact with the oxygens of the carboxylate groups as shown in the rdf for the $H(H_2S)-O$(carboxylate) pair reported in Figure 8d and illustrated in the snapshot provided in Figure 9b. Such secondary interactions could explain the presence of the low frequency asymmetric tail of the ν(SH) bands observed on this solid.

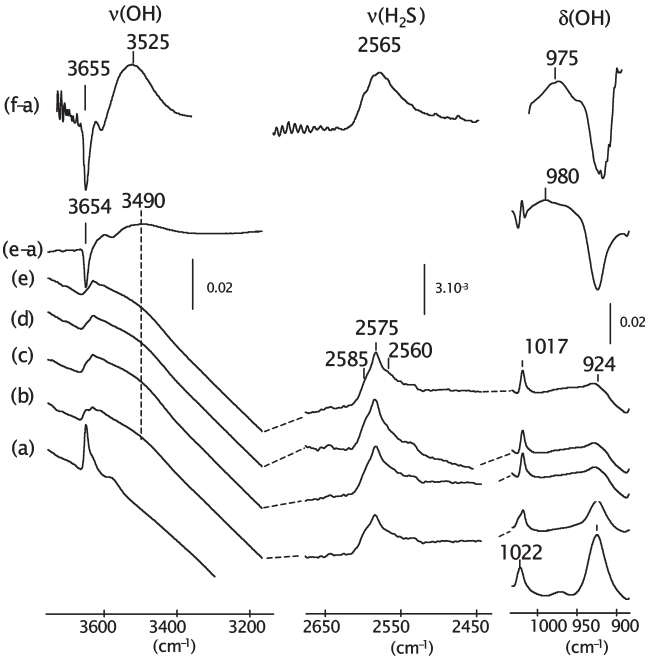

Figure 10. Infrared spectra of MIL-53(Cr) outgassed at 423 K under secondary vacuum (a) and upon increasing equilibrium H_2S pressure at room temperature ($p(H_2S)$ = 4.0 kPa (b), 13.7 kPa (c), 20.0 kPa (d), and 33.3 kPa (e)) and 220 K ($p(H_2S)$ = 4.5 kPa) (f−a).

The situation significantly differs when one analyzes the most probable arrangements of H_2S in the LP form for a loading of 10 molecules per unit cell, which corresponds roughly to the adsorbed amount experimentally obtained at the second plateau of the isotherm. As compared to the NP form, one can notice from the rdf plot (Figure 8c) that although the mean distance $S(H_2S)-H(\mu_2\text{-OH})$ is slightly shorter (2.62 Å in LP vs 2.71 Å in NP), the corresponding free energy profile calculated following the methodology described previously[28] shows a shallower well as compared to the NP form (Figure 8e). This trend is also supported by lower simulated adsorption enthalpy in the LP (-23.4 kJ·mol^{-1}) than in the NP (-32.5 kJ·mol^{-1}) structure which concurs well with those experimentally obtained via the isosteric method (-26.0 kJ·mol^{-1} and -32.0 kJ·mol^{-1}, respectively). The integration of the corresponding rdf clearly shows that all the μ_2-OH groups are involved in the interactions with H_2S via the formation of a 1:1 complex in the same way as in the NP form. Further, the interactions between H_2S and the oxygens of the carboxylate groups are much less frequent than in the NP structure. Finally, one observes in Figure 8b and Table 2 that while some weak hydrogen bonds between H_2S molecules are still present, they appear significantly weaker than in the NP form (see Figure 8b). All of the interactions in play in the LP form are summarized in the snapshots provided in Figure 9c.

CONCLUSIONS

The present combined infrared spectroscopy, gravimetry measurements, and modeling approach allowed us to successfully analyze the adsorption process of H_2S, a corrosive gas, on two Metal−Organic Frameworks materials, the flexible MIL-53(Cr) and the rigid MIL-47(V). The wavenumber of the ν18a band observed in the infrared spectra of these materials reveals that both activated materials are present in the open form. Whenever the pressure of H_2S introduced goes up to 1.8 MPa,

the MIL-47(V) structure remains rigid. By contrast, the MIL-53(Cr) shows a first structural transition from the large pore (LP) form to the narrow pore (NP) version followed by a second structural switching toward the LP structure, as already reported upon adsorption of other guest molecules including CO_2[6] and alcohols.[14] Such a result illustrates the usefulness of IR spectroscopy in the determination of structural data in the presence of corrosive gases, often difficult to explore with an in situ X-ray diffraction system due to the extreme conditions required. As shown by infrared spectroscopy, the first H_2S molecules absorbed on the MIL-53(Cr) are hydrogen-bonded to μ_2-OH groups, the hydroxyl groups playing the role of hydrogen donor. As already reported for other adsorbates, i.e., alcohols,[14] such an interaction provokes the closure of the pores at low gas or vapor loading although the Cr−OH Bronsted acid strength is low, even weaker than that of the silanol groups present on the silica surface, leading to weak hydrogen host/guest interactions. At higher loading, a full reopening of the pores occurs and H_2S molecules condense inside the pore of the LP form. The strength of the hydrogen bond of Cr−OH..SH_2 complex then becomes weaker.

To our knowledge, this is the first work that reports the experimental investigation of the adsorption sites in the MIL-47(V) material. Infrared results show that adsorption of H_2S preferentially occurs on μ_2-O atom of the V = O...V entities through hydrogen bonded species in which H_2S acts as hydrogen donor. The interaction is weak, with a calculated adsorption enthalpy of 27−29 kJ·mol^{-1}. Such a low value reveals that the basicity of these entities is weak, and so that interactions with other basic centers like oxygens of the carboxylate group and π electrons of the benzene ring can also be considered. At higher loading, the confined weakly bonded H_2S molecules form dimers, which is consistent with a liquid-like behavior.

The reversibility of H_2S adsorption at room temperature on both samples was previously established from experiments on CH_4 adsorption before and after H_2S treatment at 303 K with regeneration using primary vacuum.[5] Such a reversibility does not occur in the mesoporous type materials, i.e., MIL-100 (Cr) and MIL-101 (Cr). The comparative study was relevant as the H_2S adsorption isotherms strongly differ for both selected MILs: monotypic type I shape in the case of MIL-47(V) whereas a two-step adsorption occurs in the case of MIL-53(Cr).

In both MIL-53(Cr) and MIL-47(V), the H_2S interactions are rather weak and decrease following the sequence: MIL-53(Cr) NP > MIL-47(V) > MIL-53(Cr) LP. This behavior suggests that H_2S desorption is more difficult in MIL-53(Cr) NP than in MIL-47(V), emphasizing that this latter solid would be more appropriate for application in separation/purification processes for purifying gases containing H_2S as polutant. Preliminary simulations based on H_2S and CH_4 adsorption data on MIL-47(V) suggests a high H_2S selectivity toward CH_4 whatever the molar fraction of H_2S in the gas phase under 1.0 and 0.2 MPa, pressure which are relevant to Pressures Swing Adsorption (PSA) in industrial process.

■ ASSOCIATED CONTENT

Supporting Information. The variation of the intensity of the ν(SH) bands of adsorbed H_2S and of the δ(OH) band of the CrOH group of MIL-53(Cr) vs the H_2S pressure is presented for H_2S adsorption experiments at room temperature and at 220 K. This material is available free of charge via the Internet at http://pubs.acs.org.

■ AUTHOR INFORMATION

Corresponding Author

*E-mail: alexandre.vimont@ensicaen.fr; guillaume.maurin@univ-montp2.fr.

■ ACKNOWLEDGMENT

The Belgian authors thank the European Program of InterReg III and the financial participation of Environment and Natural Resources of the Walloon Region (Belgium). The French authors thank the CNRS and the ANR ("NoMAC" ANR-06-CO2-008) for their financial participation. L.H. thanks the Special Funds for Research (FSR) of the Faculty Polytechnique of Mons for the financial support and H.L. thanks the Lower Normandy Region Council for the financial support.

■ REFERENCES

(1) Matsuzaki, Y.; Yasuda, I. *Solid State Ionics* **2000**, *132*, 261.
(2) Cheah, S.; Carpenter, D. L.; Magrini-Bair, K. A. *Energy Fuels* **2009**, *23*, 5291.
(3) Cychosz, K. A.; Wong-Foy, A. G.; Matzger, A. J. *J. Am. Chem. Soc.* **2008**, *130*, 6938. Cychosz, K. A.; Wong-Foy, A. G.; Matzger, A. *J. Am. Chem. Soc.* **2009**, *131*, 14538.
(4) Wang, X. Q.; Liu, L. M.; Jacobson, A. J. *Angew. Chem. Int. Ed.* **2006**, *45*, 6499.
(5) Hamon, L.; Serre, C.; Devic, T.; Loiseau, T.; Millange, F.; Férey, G.; Weireld, G. D. *J. Am. Chem. Soc.* **2009**, *131*, 8775.
(6) Serre, C.; Bourrelly, S.; Vimont, A.; Ramsahye, N. A.; Maurin, G.; Llewellyn, P. L.; Daturi, M.; Filinchuk, Y.; Leynaud, O.; Barnes, P.; Férey, G. *Adv. Mater.* **2007**, *19*, 2246.
(7) Serre, C.; Millange, F.; Thouvenot, C.; Nogues, M.; Marsolier, G.; Louer, D.; Férey, G. *J. Am. Chem. Soc.* **2002**, *124*, 13519.
(8) Barthelet, K.; Marrot, J.; Riou, D.; Férey, G. *Angew. Chem. Int. Ed.* **2002**, *41*, 281.
(9) Millange, F.; Serre, C.; Férey, G. *Chem. Commun.* **2002**, 822.
(10) Loiseau, T.; Serre, C.; Huguenard, C.; Fink, G.; Taulelle, F.; Henry, M.; Bataille, T.; Férey, G. *Chem.—Eur. J.* **2004**, *10*, 1373.
(11) Vimont, A.; Travert, A.; Bazin, P.; Lavalley, J. C.; Daturi, M.; Serre, C.; Férey, G.; Bourrelly, S.; Llewellyn, P. L. *Chem. Commun.* **2007**, 3291.
(12) Horcajada, P.; Serre, C.; Maurin, G.; Ramsahye, N.; Balas, F.; Vallet-Regi, M.; Sebban, M.; Taulelle, F.; Férey, G. *J. Am. Chem. Soc.* **2008**, *130*, 6774.
(13) Hamon, L.; Llewellyn, P. L.; Devic, T.; Ghoufi, A.; Clet, G.; Guillerm, V.; Pirngruber, G. D.; Maurin, G.; Serre, C.; Driver, G.; Beek, W. v.; Jolimaitre, E.; Vimont, A.; Daturi, M.; Férey, G. *J. Am. Chem. Soc.* **2009**, *131*, 17490.
(14) Bourrelly, S.; Moulin, B.; Rivera, A.; Maurin, G.; Devautour-Vinot, S.; Serre, C.; Devic, T.; Horcajada, P.; Vimont, A.; Clet, G.; Daturi, M.; Lavalley, J. C.; Loera-Serna, S.; Denoyel, R.; Llewellyn, P. L.; Férey, G. *J. Am. Chem. Soc.* **2010**, *132*, 9488.
(15) Devic, T.; Horcajada, P.; Serre, C.; Salles, F.; Maurin, G.; Moulin, B.; Heurtaux, D.; Clet, G.; Vimont, A.; Greneche, J. M.; Le Ouay, B.; Moreau, F.; Magnier, E.; Filinchuk, Y.; Marrot, J.; Lavalley, J. C.; Daturi, M.; Férey, G. *J. Am. Chem. Soc.* **2010**, *132*, 1127.
(16) Bourrelly, S.; Llewellyn, P. L.; Serre, C.; Millange, F.; Loiseau, T.; Férey, G. *J. Am. Chem. Soc.* **2005**, *127*, 13519.
(17) Rosenbach, N.; Ghoufi, A.; Deroche, I.; Llewellyn, P. L.; Devic, T.; Bourrelly, S.; Serre, C.; Férey, G.; Maurin, G. *Phys. Chem. Chem. Phys.* **2010**, *12*, 6428.
(18) Dreisbach, F.; Staudt, R.; Tomalla, M.; Keller, J. U. *Fundamentals of Adsorption*; 5th International Conference on Fundamentals of Adsorption, 1995, Asilomar, CA.
(19) Le Van, M. D.; Kluwer Academic Publishers: Boston, MA, 1996, 259.

(20) De Weireld, G.; Frère, M.; Jadot, R. *Meas. Sci. Technol.* **1999**, *10*, 117.
(21) Frère, M.; De Weireld, G.; Jadot, R. *Fundamentals of Adsorption*; 6th International Conference on Fundamentals of Adsorption, 1998, Presqu'île de Giens, France.
(22) Dreisbach, F.; Seif, R.; Losch, H. W. *J. Therm. Anal. Calorim.* **2003**, *71*, 73.
(23) Belmabkhout, Y.; Frère, M.; De Weireld, G. *Meas. Sci. Technol.* **2004**, *15*, 848.
(24) (a) Rouquerol, F.; Rouquerol, J.; Sing, K. *Adsorption by Powders and Porous Solids*; Academic Press: London, 1999.(b) Llewellyn, P. L.; Maurin, G. C.R. *Chimie* **2005**, *8*, 283.
(25) McCarthy, R. D.; Arp, V. D. *Adv. Cryo. Eng.* **1990**, *35*, 1465.
(26) Lemmon, E. W.; Span, R. J. *J. Chem. Eng. Data* **2006**, *51*, 785.
(27) Nokerman, J.; Canet, X.; De Weireld, G.; Frere, M. *Adsorption* **2005**, *11*, 121.
(28) Salles, F.; Ghoufi, A.; Maurin, G.; Bell, R. G.; Mellot-Draznieks, C.; Férey, G. *Angew. Chem., Int. Ed.* **2008**, *47*, 8487.
(29) Rappe, A. K.; Casewit, C. J.; Colwell, K. S.; Goddard, W. A.; Skiff, W. M. *J. Am. Chem. Soc.* **1992**, *114*, 10024.
(30) Mayo, S. L.; Olafson, B. D.; Goddard, W. A. *J. Phys. Chem.* **1990**, *94*, 8897.
(31) Ramsahye, N. A.; Maurin, G.; Bourrelly, S.; Llewellyn, P. L.; Loiseau, T.; Serre, C.; Férey, G. *Chem. Commun.* **2007**, 3261.
(32) Ramsahye, N. A.; Maurin, G.; Bourrelly, S.; Llewellyn, P. L.; Devic, T.; Serre, C.; Loiseau, T.; Férey, G. *Adsorption* **2007**, *13*, 461.
(33) Kamath, G.; Lubna, N.; Potoff, J. J. *J. Chem. Phys.* **2005**, *123*, 124505.
(34) Widom, B. *J. Chem. Phys.* **1963**, *39*, 2808.
(35) Vlugt, T. J. H.; Garcia-Perez, E.; Dubbeldam, D.; Ban, S.; Calero, S. *J. Chem. Theory Comput.* **2008**, *4*, 1107.
(36) Ault, B. S. *J. Mol. Struct.* **2000**, *526*, 97.
(37) Saumagne, P.; Dorval, P. *C. R. Acad. Sci., Ser. B* **1966**, *263*, 963.
(38) Tsujii, H.; Takizawa, K.; Koda, S. *Chem. Phys.* **2002**, *285*, 319.
(39) Jorgensen, W. L. *J. Phys. Chem.* **1986**, *90*, 6379.
(40) Travert, A.; Manoilova, O. V.; Tsyganenko, A. A.; Mauge, F.; Lavalley, J. C. *J. Phys. Chem. B* **2002**, *106*, 1350.
(41) Garcia, C. L.; Lercher, J. A. *J. Phys. Chem.* **1992**, *96*, 2230.